SAND2014-0466C

Multispectral sorter for rapid, nondestructive optical bioprospecting for algae biofuels

Ryan W. Davis, Hauwen Wu, Seema Singh

Sandia National Laboratories, Livermore, CA USA
Joint BioEnergy Institute, Emeryville, CA, USA

ABSTRACT

Microalgal biotechnology is a nascent yet burgeoning field for developing the next generation of sustainable feeds, fuels, and specialty chemicals. Among the issues facing the algae bioproducts industry, the lack of efficient means of cultivar screening and phenotype selection represents a critical hurdle for rapid development and diversification. To address this challenge, we have developed a multi-modal and label-free optical tool which simultaneously assesses the photosynthetic productivity and biochemical composition of single microalgal cells, and provides a means for actively sorting attractive specimen (bioprospecting) based on the spectral readout. The device integrates laser-trapping micro-Raman spectroscopy and pulse amplitude modulated (PAM) fluorometry of microalgal cells in a flow cell. Specifically, the instrument employs a dual-purpose epi-configured IR laser for single-cell trapping and Raman spectroscopy, and a high-intensity VIS-NIR trans-illumination LED bank for detection of variable photosystem II (PSII) fluorescence. Micro-Raman scatter of single algae cells revealed vibrational modes corresponding to the speciation and total lipid content, as well as other major biochemical pools, including total protein, carbohydrates, and carotenoids. PSII fluorescence dynamics provide a quantitative estimate of maximum photosynthetic efficiency and regulated and non-regulated non-photochemical quenching processes. The combined spectroscopic readouts provide a set of metrics for subsequent optical sorting of the cells by the laser trap for desirable biomass properties, e.g. the combination of high lipid productivity and high photosynthetic yield. Thus the device provides means for rapid evaluation and sorting of algae cultures and environmental samples for biofuels development.

Keywords. cell sorting, laser trap, micro-Raman, PAM fluorometry, algae biofuels

1. INTRODUCTION

Microalgae have long been of interest as a potential source of biofuel based on the observation that certain species of algae can accumulate large quantities of biomass and energy dense lipids when grown under specific environmental conditions [1, 2]. The primary conclusion of multiple techno-economic feasibility analyses suggests that high lipid composition microalgal biomass is paramount for approaching price parity with the established liquid fuels industry [3, 4]. However, strains or conditions that optimize lipid enrichment by sacrificing photosynthetic productivity are unacceptable for realization of algae-based biodiesel. Recently, the number of

algal strains world-wide was conservatively estimated to be 72,500 species, although the actual number may be greater than an order of magnitude higher [5]. Among these, only a very minor fraction have been characterized to any level of detail, and current estimates of the primary biomass productivity of common algal production strains is approximately one third of the requirement for sustainable algal biodiesel production at large scale [6]. Clearly, efficient and accurate analysis, screening, and selection of the most productive cells represents a critical hurdle for rapid progress toward algae-based biofuels.

Most commonly the lipid content of microalgae is analyzed by solvent extraction and chromatography [7]. This approach provides compositional identification of the extracted lipids but is relatively time-, chemical- and labor-intensive. Moreover, this and similar methods lose information that connects metabolic processes of single cells to optimal lipid production because they require destructive homogenization of large amounts of cells. This defeats the goal of identifying the best-producers, cloning and cultivating them, and potentially genetically manipulating them to create even more-productive cells with desired traits [8]. Fluorescent probes (e.g. Nile red, Bodipy) can allow single-cell lipid analyses, but these approaches are limited because they can be toxic to some species of microalgae. Also their fluorescence intensity can be influenced by other pigments in algae and dye uptake varies in different species, leading to inaccuracies. Furthermore, these approaches provide little chemical information about the lipids, such as the composition, melting temperature, degree of unsaturation (number and location of carbon-carbon double bonds), and chain length (number of carbon atoms forming the molecular backbone of the lipid). They also do not provide other compositional information about the cells, nor their rate of photosynthetic conversion of solar energy to biomass. All these properties are crucially important to the quality and productivity of the biodiesel derived from these lipids, and therefore determine which algal species and which cultivation methods for that species are the optimal combination. Common methods of algal screening predominantly rely on measurements of bulk properties (those from a statistical analysis of a population of cells), effectively eliminating the possibility for selecting the highest performing cells from a single culture or algal strain.

In summary, one of the greatest challenges in current microalgal research is to rapidly analyze, discover, and cultivate (or "fingerprint") species and strains of algae that can most efficiently and productively transform solar energy into lipids that can readily be converted into biodiesel or other types of transportation fuels. In this manuscript we detail the results of our recent efforts to develop an optical cell sorter that combines measurements of lipid and photosynthetic productivities for rapid algae cultivar screening and selection. The effort builds on our recent observations of algal lipid enrichment using hyperspectral confocal fluorescence microscopy (HCFM) [9] and laser trap Raman spectroscopy (LTRS) [10].

2. MATERIALS AND METHODS

2.1 Optical design and system calibration

The optical system for the multispectral sorter combines an optical trap, a micro-Raman system with a confocal pinhole, an amplitude-modulated fluorometer, and a microfluidic Y-chip (channel diameter = 150 μm) connected to syringe pump in a single custom-built configuration (see Figure 1). The micro-Raman system consists of a 785-nm laser with 70-mW output power

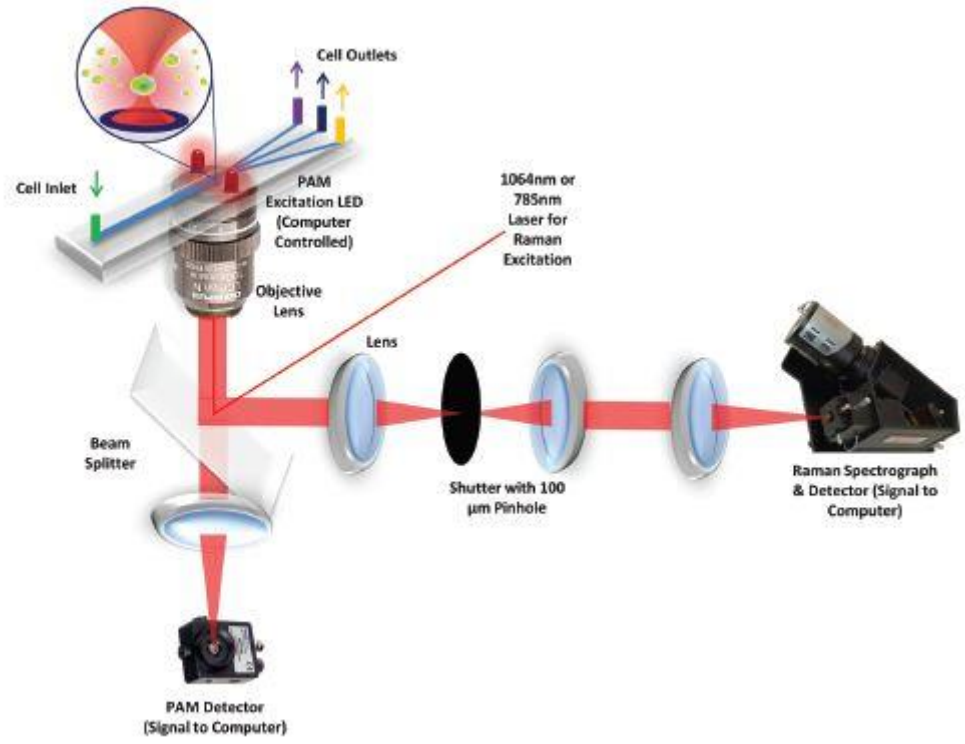

Figure 1. Cartoon schematic of the multispectral bioprospector apparatus.

from a continuous-wave diode-pumped solid-state laser (CrystaLaser) was directed through a 4× beam expander and a 785-nm bandpass filter (Omega Filters) to remove any additional plasma emission generated within the laser tube. The beam was then delivered into an inverted Olympus optical microscope (IX71), equipped with a dichroic shortpass beamsplitter (Chroma Technology) to reflect the laser beam into a 1.2 N.A. 60× water-immersion objective lens, resulting in a diffraction limited spot of 0.5-µm diameter at the laser focus. The beam was focused through microfluidic channel with a power of ~10 mW out of the objective. Raman scattering generated at the focus was collected by the same objective, passed through the dichroic beamsplitter and a longpass edge filter (Omega Filters) to block elastic scattering photons, and then focused through a 100-µm pinhole for background signal rejection. The signal is dispersed by a spectrometer (Acton 2300i; Princeton Instruments) equipped with 1-µm blaze wavelength 300 g/cm grating and projected on an air-cooled EM-CCD with 1,340 × 100 pixels (PIXIS; Roper Scientific). Spectral resolution was 3 cm^{-1} (3,200 cm^{-1}/1,280 pixels).

Using the same optical train, excitation modulated fluoresce is excited using trans-illumination from an 3W 620-630 nm LED (Cree XPE Red), filtered for detection of chlorophyll emission using a 660-700 nm bandpass filter (Semrock, Inc.), and focused on a Si photodiode (S1087, Hamamatsu) as depicted in Figure 1. An additional far-red LED (3W, 730 nm, Cree) is positioned at a 45° from the sample and employed for rapid reoxidation of the PSII acceptor pool following the photosynthetic yield assessment. Excitation modulation was achieved using an embedded digital potentiometer programmed for interleaving 1 msec duration saturation pulses with incrementally stepped actinic (photosnythetically active radiation, PAR) illumination,

adapted from the rapid light scanning pulse amplitude modulated fluorometry (RLS-PAM) routine described by White and Critchley [11]. Calibration of the RLS-PAM illumination was performed using a spherical micro-quantum sensor (US-SQS/L, Walz GmbH) positioned at the sample interface in order to obtain an actinic photon flux range of 50 – 1600 μmol/m^2/sec, and a saturation photon flux of 15,000 μmol/m^2/sec. Calibration of the Raman emission wavelength was performed using a hollow-cathode Kr^+ ion lamp, and dark spectra were used to correct for background signals and instrument offset.

A spectral library of model algae lipids was prepared from Raman spectra of several single fatty acids typically found in algal lipid extracts, as described in Wu et al [10]. Briefly, Raman bands corresponding to (*i*) the ═C—H *cis* stretch at 1,260 cm^{-1}, (*ii*) the C═C stretch at 1,650 cm^{-1}, and (*iii*) the ═C—H stretch at 3,023 cm^{-1} provide unequivocal evidence for chain unsaturation. Second, the presence and relative intensities of C—C *gauche* stretch at 1,075 cm^{-1} and C—C *trans* stretches at 1,056 cm^{-1} and 1,116 cm^{-1} can be used to assess the phase state of the constituent lipids because fatty acid tails are packed in an orderly *trans* conformation in the solid phase, whereas *gauche* conformers populate the more disordered, fluid phases [12]. Third, peaks assigned to saturated CH_2 bonds, such as the CH_2 twist at 1,300 cm^{-1}, the CH_2 bend at 1,440 cm^{-1}, and the CH_2 symmetric and asymmetric stretches at ∼2,800–3,000 cm^{-1}, are typically strong in saturated fatty acids. For instance, between arachidonic acid (20:4, T_m = −50 °C) and stearic acid (18:0, T_m = 70 °C), the unsaturation markers, 1,260 cm^{-1}, 1,650 cm^{-1}, and 3,023 cm^{-1} consistently diminish, whereas the relative intensities of the bands related to the CH_2 bond increase. The *gauche* conformers are gradually suppressed and intensities caused by *trans* conformers increase for lipids with higher T_m. These markers provide a semiquantitative classification for the presence and concentration of specific lipid types in unknown samples. Semiquantitative information related to the chain length, unsaturation, and T_m can be deduced from the Raman spectra; information typically inaccessible in fluorescence-based data.

2.2 Data acquisition

The process of evaluating and sorting cells requires basic coordination of hardware and software. In the initial state of the device, the trapping laser is “on” and the RLS-PAM actinic LED is at low intensity. Dark adapted algal cells are fluidically transported from the syringe pump to the microfluidic chip containing optical probe volume. The flow rate of the microalgae suspension depends on the concentration of the cells in the medium, however optimization of the flow velocity did not significantly improve the overall through-put of the device unless the sample was very dilute. In the probe volume, an individual cell is captured in the IR beam and illuminated by the RLS-PAM actinic LED, resulting in a chlorophyll fluorescence signal at the photodiode. The flow is then suspended via triggering based on an increase in the output of the photodiode of >10x background. The optical trap positions the cell several micrometers from the walls of the microfluidic well to avoid interfacial perturbations. Signals from regions outside

the sample point are rejected by the confocal pinhole, affording high signal-to-noise ratio needed for single-cell Raman spectroscopy. Typical acquisition times for well-resolved spectra of algal cells were found to be ~10 s. Although lipid characterization relies on static accumulation of the Raman scattering signal and photosynthetic characterization relies on a temporally variable fluorescence response to intensity modulated excitation, the total time scales of the two measurements affords a two-level photosynthetic yield assessment. For this assessment, fluorescence intensity data is collected at the low photon flux excitation (50 μmol/m^2/sec, 1 sec) followed by a saturation excitation pulse (15000 μmol/m^2/sec, 1 msec), a subsequent increased photon flux excitation (1000 μmol/m^2/sec, 4 sec) followed by a second saturation excitation pulse, and a final low photo flux excitation (50 μmol/m^2/sec, 4 sec) followed by 1 sec exposure to the far red LED. After the 10 sec combined optical interrogation, the data is processed and the cell is retained or rejected based on user-defined parameters and actuated by the combination of galvo-based deflection of the laser and resumption of fluid flow.

2.3 Data analysis

Analysis of the micro-Raman data was performed using the ratiometric methods described in Wu, et al [10] for quantitative analysis of degree of unsaturation, carbon chain length, and phase transition temperature (T_m) of the cellular lipids. Briefly, the method uses the linear correlation between the intensities of the 1650 cm^{-1} (I_{1650}) and 1440 cm^{-1} (I_{1440}) to establish the number of degrees of unsaturation, the ratio of saturated and unsaturated carbons, and the T_m based on the the model lipid library described above. Multiplication of the values obtained for degree of unsaturation and ratio of saturated to unsaturated bonds provides the overall carbon chain length. Ratiometric comparison of the I_{1440} and the I_{1007} provides an additional estimate of the total lipid:protein for each cell.

Analysis of the RLS-PAM data for estimation of maximum photosynthetic yield, photosynthetic energy utilization, and regulated and unregulated photochemical quenching parameters was performed as described previously using the Stern-Volmer approach [13, 14]. Briefly, under dark adaptation conditions, the average fluorescence intensity obtained under the initial (1 sec) low photon flux excitation provides the dark fluorescence yield (F_0). The maximum fluorescence yield (F_m) is obtained from the fluorescence plateau obtained during the brief saturation pulse. The maximum PSII quantum yield (F_v/F_m) is obtained from the equation,

$$F_v/F_m = (F_m - F_0)/F_m \ .$$

Following the initial PAR exposure, the subsequent elevated photon flux excitation provides the effective PSII quantum yield, *Y(II)*, obtained by the previous expression, with $F_m = F_m'$, ie. the modified F_m obtained at the fluorescence plateau during the second saturation pulse, and $F_0 = F$, ie. the modified F_0 obtained under increased, physiologically relevant PAR intensity (50-1600 μmol/m^2/sec photon flux). The non-photochemical quenching parameter, *NPQ*, is calculated

according to a diffusion-limited Stern-Volmer quenching mechanism using the aforementioned fluorescence parameters according to the equation,

$$NPQ = (F_m - F_m')/F_m' .$$

The effective PSII quantum yield, *Y(II)*, sums to unity with the regulated, *Y(NPQ)*, and unregulated, *Y(NO)*, energy dissipation mechanisms to account for the PAR absorption in PSII. The coefficient of photochemical quenching, *qL*, required for differentiation of the two energy dissipation mechanisms is obtained following exposure to the far red illumination to obtain the minimal fluorescence yield, F_0', and the aforementioned effective PSII quantum yield parameters according to the equation,

$$qL = F_0'(F_m' - F)/(FF_m' - FF_0')$$

Finally, *Y(NO)* and *Y(NPQ)* are calculated using the following equation, and by incorporating the unity constrain among these parameters and *Y(II)*.

$$Y(NO) = (1 + NPQ + qL(F_m/F_0 - 1))^{-1}$$

3. RESULTS

Previously, the temperature of trapped cells in a large reservoir of aqueous buffer was found to be stable near the bath temperature [15], in this case, room temperature. However, because the current apparatus incorporates a microfluidic well format, we sought to confirm the cell viability following confined laser-trapping conditions. Confinement of biflagellate *C. reinhardtii* cells – noted for their relative fragility – for durations of 1min inside the laser trap yielded no loss of apparent motility following termination of the assay, suggesting that the system has minimal negative impact on the health state of the cells.

In order to assess the sensitivity of the apparatus to the abiotic factors impacting the combination of photosynthetic and lipid productivities, the multispectral sorter apparatus was tested using monocultures of the common micoralgal production strain, *Dunaiella salina,* cultured at a range of salinities from ~0.5M to 2.5M. Because of the species' importance for nutraceutical and feed applications [16, 17], *D. salina* provides a well-studied model for microalgal bioprospecting. Most important for this application, *D. salina* exhibits the somewhat remarkable property of increased photosynthetic yield [18] and a correlated increase in elongated and unsaturated lipids under high salinity regimes [19]. Figure 2 depicts hyperspectral confocal fluorescence images of single *D. salina* cells cultures at high PAR (275 μmol/m^2/sec photon flux) and three varying salinity levels (HS: high salt, MS: moderate salt, and LS: low salt).

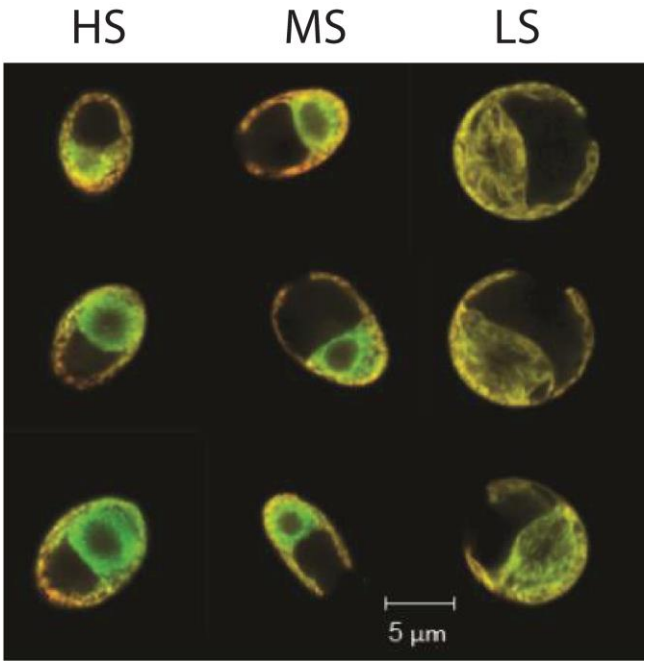

Figure 2. Hyperspectral confocal fluorescence images of *Dunaliella salina* cultivated in a variety of salinity media (LS = 0.5M, MS = 1.5M, HS = 2.5M NaCl). Two dominant spectral components, corresponding to a single chlorophyll fluorescence peak (green, emission max 681 nm), and a broad carotenoid fluorescence (red, 520-600 nm superimposed with sharp resonance Raman peaks) are depicted.

In addition to clear morphological differences in the cells, including cell roundness and effective volume, the cells display distinct differences in the intensity and localization of the two dominant spectral components. The chloroplast spectral component (green) is characterized by a high intensity chlorophyll-a emission (peak at ~680 nm) colocalized with low levels of carotenoid emission; the carotenoid spectral component (red) is characterized by a minor, but broad chlorophyll fluorescence (~660-680 nm) with high levels of carotenoid emission (~520-600 nm). Sharp peaks were observed in these spectra and attributed to resonance enhanced Raman scattering observed previously using hyperspectral confocal fluorescence imaging of cyanobacteria [20]. The Raman bands were assigned to three major vibrational modes of carotenoids, the C=C stretch (1529±10 cm^{-1} or 527 nm), the C-C stretch (1157±10 cm^{-1} or 519 nm), and a C-C bend (1004±10 cm^{-1} or 514 nm). Although progressive shifts in the wavenumber of the C=C stretching band are correlated to increased polyene chain length, deviations in the exact frequency shift should be expected by interactions with the host matrix [21]. The observation of resonance enhanced Raman emission from these components is likely indicative of their role in regulated non-photochemical quenching via dissipation of excess excitation energy as heat through the molecular vibrations.

Figure 3 depicts tandem micro-Raman and RLS-PAM data collected using the multispectral bioprospector apparatus. In this test case, characteristic Raman spectra and photosynthetic parameters were obtained with minimal impact on the overall signal-to-noise ratios observed in either stand-alone measurement. Furthermore, the averaged data from the measurement recapitulates the previous observations from other laboratories and provides additional, previously unkown details related to the single-cell variance of the photosynthetic and lipid yield parameters under the various salinity conditions.

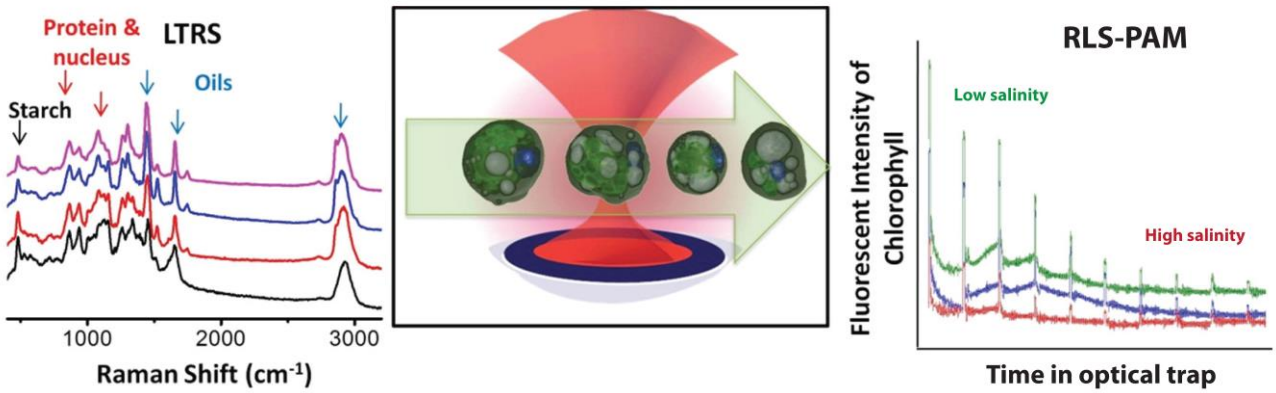

Figure 3. Simultaneous collection of Raman spectra and PSII yields from single laser-trapped algae cells cultured in media of varying salinity.

Figure 4 depicts correlations among the major measured parameters for 50 individual cells from each culture condition. In figure 4(A), average lipid carbon chain lengths and degree of unsaturation of the lipids is shown for the various salinity regimes. At the low salinity regime, the average carbon chain length was 16.07, variance 0.367; at the medium salinity regime the average was 16.32, variance 0.444; and at the high salinity regime the average was 16.38, variance 0.496. At the low salinity regime, the average single cell degree of lipid unsaturation was 1.24, variance 0.013; at the medium salinity regime the average was 1.55, variance 0.038; and at the high salinity regime the average was 1.68, variance 0.083. To our knowledge this is the first report indicating increased cell-to-cell variance in the carbon chain length (135%) and degree of lipid unsaturation (638%) at increasing salinities in *Dunaliella salina*. In figure 4(B), the total lipid to protein ratio is plotted against the single-cell maximum (dark adapted) photosynthetic yield. At the low salinity regime, the maximum photosynthetic yield (F_v/F_m) was 56.6%, variance 0.0102%; at the medium salinity regime the F_v/F_m was 58.0%, variance 0.0095%; and at the high salinity regime the F_v/F_m was 60.9%, variance 0.0080%. At the low salinity regime, the lipid:protein was 1.67, variance 0.09; at the medium salinity regime the lipid:protein was 0.438, variance 0.047; and at the high salinity regime the lipid:protein was 0.91, variance 0.065. From this plot a correlation between high lipid:protein and reduced photosynthetic yield is apparent, although several outliers with simultaneously high lipid:protein and photosynthetic yield were detected. Furthermore, the single cell correlations between the photosynthetic yield and lipid:protein appear to provide reasonably high fidelity classification for the salinity adapted state of the cells.

4. DISCUSSION

A recent assessment of biofuels production capacity (i.e. bioethanol and biodiesel) from microalgae suggests that the optimal composition of the biomass should approach 60% lipids, 30% starch, and 10% protein [22]. Although there are many reports of algae biomass with compositions that compare favorably to these, typically such samples are produced using a nutrient-deprivation based lipid enrichment phase which often correlates to dramatically decreased overall growth yields [9]. Clearly, approaches that can rapidly identify single-cell outliers for propagation based on high productivity and lipid accumulation would be useful for accelerating development of algae biofuels. In this manuscript we describe an optical platform, dubbed multispectral bioprospector, which uses laser trapping of single cells for simultaneous assessment of photosynthetic yield parameters and biochemical composition. Single cell photosynthetic yields were collected using a RLS-PAM modified for collection of the maximum photosynthetic yield, effective photosynthetic yield at a user-specified PAR flux (in this case 1000 μmol/m^2/sec), and the corresponding regulated and unregulated non-photochemical quenching parameters at the stated PAR flux in ~10 sec. This approach extends the typical RLS-PAM routine [14] to single cells and shortens the duration of the full measurement by a factor of 20-50x to coincide with a high signal-to-noise single-cell micro-Raman measurement. Single cell micro-Raman provides high lipid specificity, but also provides an estimation of protein and carbohydrate content for evaluation of the mass balance parameter identified in Ref 22 above.

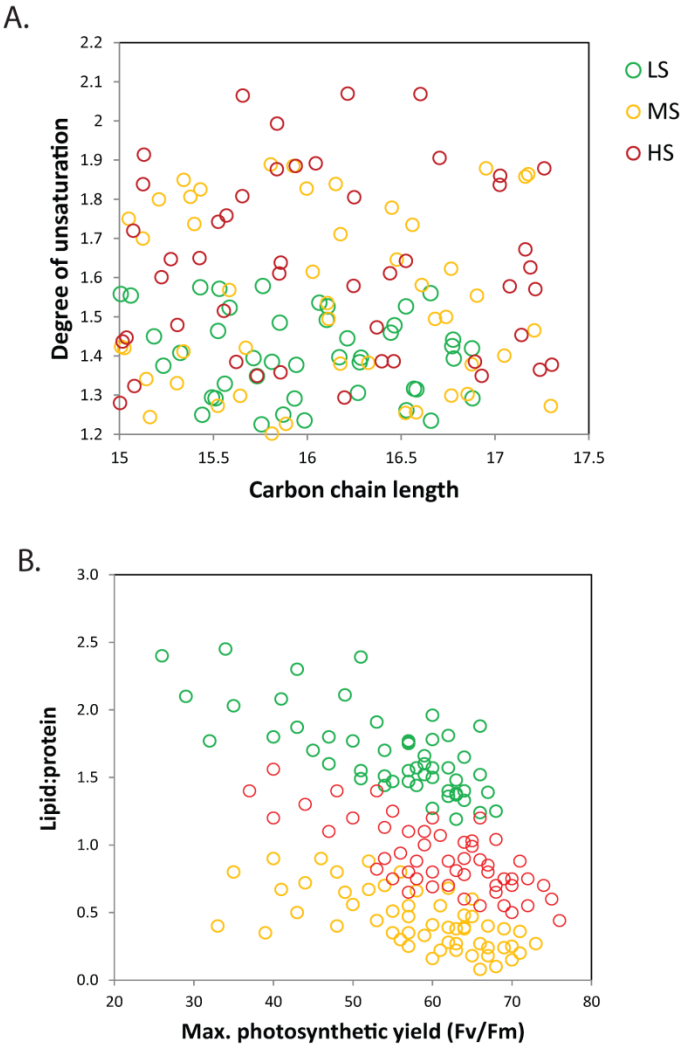

Figure 4. Single-cell parameters obtained from the multispectral bioprospector apparatus. A) Correlation between fatty acid carbon chain length and degree of unsaturation for *D. salina* cultivated at various salinity regimes (LS: low salt, MS: medium salt, HS: high salt). B) Correlation of the maximum photosynthetic yield and lipid:protein obtained from RLS-PAM and LTRS, respectively.

For this application, we sought to demonstrate the function of the multispectral bioprospector for cultivar screening of *Dunaliella salina* under various salinity regimes. Specifically, we hoped to identify lipid yield and photosynthetic parameters for subsequent

isolation of attractive cultivar parent cells. The results confirm a previous work that found increased lipid chain elongation and lipid saturation under increased salinity [19], however, our data suggest that the variance in these parameters also increases substantially at elevated salinity (up to 2.5M). Furthermore, our results confirm a previous report of increased photosynthetic yield at increased salinity [18], and further show that lipid productivity is typically anticorrelated with photosynthetic yield. Among the data, subsets of single cell outliers were identified that could support directed evolution towards a high lipid, high productivity strain for biofuels. Specifically, for cells grown at low salinities, a few individuals with maximum photosynthetic yield >67% and lipid:protein >1.8 were identified. Although the number of such cells was low (~1 in 50), isolation of 10 such members for propagation could be achieved in ~15 minutes based on the throughput of the device at moderately high culture densities. Although these results specifically focused on a single algae species with an abiotic culture variable (salinity), we expect that the method and algorithms should be broadly applicable to natural assemblages of microalgae and cyanobacteria and for screening of genetically modified organisms.

5. REFERENCES

[1] J. Sheehan, T. Dunahay, J. Benemann *et al.*, [Look Back at the U.S. Department of Energy's Aquatic Species Program: Biodiesel from Algae; Close-Out Report], (1998).

[2] Y. Chisti, "Biodiesel from microalgae," Biotechnology Advances, 25, 294-306 (2007).

[3] Q. Hu, M. Sommerfeld, E. Jarvis *et al.*, "Microalgal triacylglycerols as feedstocks for biofuel production: perspectives and advances," Plant J, 54(4), 621-39 (2008).

[4] P. T. Pienkos, and A. Darzins, "The promise and challenges of microalgal-derived biofuels," Biofuels Bioproducts & Biorefining-Biofpr, 3(4), 431-440 (2009).

[5] M. D. Guiry, "How many species of algae are there?," Journal of Phycology, 48(5), 1057-1063 (2012).

[6] R. Davis, D. Fishman, E. D. Frank *et al.*, [Renewable diesel from algal lipids: An integrated baseline for cost, emissions, and resource potential from a harmonized model], (2012).

[7] J. Jones, S. Manning, M. Montonya *et al.*, "Extraction of algal lipids and their analysis by HPLC and mass spectrometry," J Am Oil Chem Soc, 89(8), 1371-1381 (2012).

[8] R. Radakovits, R. E. Jinkerson, A. Darzins *et al.*, "Genetic engineering of algae for enhanced biofuel production," Eukaryotic Cell, 9(4), 486-501 (2010).

[9] R. W. Davis, J. V. Volponi, H. D. Jones *et al.*, "Multiplex fluorometric assessment of nutrient limitation as a strategy for enhanced lipid enrichment and harvesting of Neochloris oleoabundans," Biotechnol Bioeng, 109(10), 2503-12 (2012).

[10] H. Wu, J. V. Volponi, A. E. Oliver *et al.*, "In vivo lipidomics using single-cell Raman spectroscopy," Proc Natl Acad Sci U S A, 108(9), 3809-14 (2011).

[11] A. J. White, and C. Critchley, "Rapid light curves: A new fluorescence method to assess the state of the photosynthetic apparatus," PHotosynthesis Research, 59(1), 63-72 (1999).

[12] J. L. Lippert, and W. L. Peticolas, "Laser Raman investigation of the effect of cholesterol on conformational changes in dipalmitoyl lecithin multilayers," Proc Natl Acad Sci U S A, 68, 1572-1576 (1971).

[13] U. Schreiber, [Pulse-amplitude (PAM) fluorometry and saturation pulse method] Kluwer Academic Publishers, Dordecht, The Netherlands(2004).

[14] D. M. Kramer, G. Johnson, O. Kiirats *et al.*, "New fluorescence parameters for the determination of Qa redox state and excitation energy fluxes," Photosynthesis Research, 79, 209-218 (2004).
[15] H. Mao, J. R. Arias-Gonzalez, S. B. Smith *et al.*, "Temperature control methods in a laser tweezers system," Biophys J, 89(2), 1308-1316 (2005).
[16] A. Ben-Amotz, and M. Avron, [The potential use of Dunaliella for the production of glycerol, b-carotene, and high-protein feed] Plenum Pub. Corp., New York(1982).
[17] T. P. Moulton, L. J. Borowitzka, and D. J. Vincent, "The Mass-Culture of Dunaliella-Salina for Beta-Carotene - from Pilot-Plant to Production Plant," Hydrobiologia, 151, 99-105 (1987).
[18] A. J. Liska, A. Shevchenko, U. Pick *et al.*, "Enhanced photosynthesis and redox energy production contribute to salinity tolerance in Dunaliella as revealed by homology-based proteomics," Plant Physiol, 136(1), 2806-17 (2004).
[19] M. Azachi, A. Sadka, M. Fisher *et al.*, "Salt induction of fatty acid elongase and membrane lipid modifications in the extreme halotolerant alga Dunaliella salina," Plant Physiol, 129(3), 1320-9 (2002).
[20] W. F. J. Vermaas, J. A. Timlin, H. D. T. Jones *et al.*, "In vivo hyperspectral confocal fluorescence imaging to determine pigment localization and distribution in cyanobacterial cells," Proceedings of the National Academy of Sciences of the United States of America, 105(10), 4050-4055 (2008).
[21] V. E. de Oliveira, H. V. Castro, H. G. M. Edwards *et al.*, "Carotenes and carotenoids in natural biological samples: a Raman spectroscopic analysis," Journal of Raman Spectroscopy, 41(6), 642-650 (2010).
[22] M. Martin, and I. E. Grossmann, "Optimal engineered algae composition for the integrated simultaneous production of bioethanol and biodiesel," AIChE Journal, 59(8), 2872-2883 (2013).